Physics Letters B 837 (2023) 137655

Contents lists available at ScienceDirect

Physics Letters B

journal homepage: www.elsevier.com/locate/physletb

Multi-modal mass-asymmetric fission of ^{178}Pt from simultaneous mass-kinetic energy fitting

B.M.A. Swinton-Bland [a,*], J. Buete [a], D.J. Hinde [a], M. Dasgupta [a], T. Tanaka [a], A.C. Berriman [a], D.Y. Jeung [a], K. Banerjee [a,1], L.T. Bezzina [a], I.P. Carter [a], K.J. Cook [a], C. Sengupta [a,2], C. Simenel [a,b], E.C. Simpson [a], M.A. Stoyer [a,c]

[a] Department of Nuclear Physics and Accelerator Applications, Research School of Physics, Australian National University, Canberra, ACT 2601, Australia
[b] Department of Fundamental and Theoretical Physics, Research School of Physics, Australian National University, Canberra, ACT 2601, Australia
[c] Nuclear and Chemical Sciences Division, Lawrence Livermore National Laboratory, Livermore, CA 94550, USA

ARTICLE INFO

Article history:
Received 26 September 2022
Received in revised form 16 December 2022
Accepted 28 December 2022
Available online 3 January 2023
Editor: D.F. Geesaman

Keywords:
Nuclear fission
Neutron-deficient nuclei
Mass-asymmetric fission
Deformed shell gaps
Sub-lead fission
Mass-kinetic energy

ABSTRACT

The observation of mass-asymmetric fission in neutron-deficient ^{180}Hg dramatically expanded the region of mass-asymmetric fission found across the nuclide chart, and has led to intense experimental and theoretical investigations into the fission of sub-lead nuclei. In particular, two major questions have been raised: how many fission modes are present in the fission of sub-lead nuclides, and which shells dictate these modes?

Notably, investigations of the fission modes of ^{178}Pt have led to contrasting results. To solve this disparity, new high-statistics data have been measured at the lowest excitation energy to-date using the CUBE fission spectrometer at The Australian National University. A new fitting procedure was developed to fit the high-statistics two-dimensional mass-kinetic energy distribution without external constraints.

The fission of ^{178}Pt can best be described by three fission modes: one mass-symmetric and two mass-asymmetric. Comparisons to previous analyses highlight the necessity of fitting the two-dimensional mass-kinetic energy distribution, rather than fitting slices of individual one-dimensional projections of the full distribution. Systematic studies of high-statistics measurements, combined with a rigorous statistical analysis offer the best chance to determine the shell effects responsible for multi-modal mass-asymmetric fission in this region of the nuclide chart.

1. Introduction

Nuclear fission, the division of a single nucleus into two fragments, is one of the least understood fundamental processes in nuclear physics. Whilst the macroscopic liquid drop model (LDM) provided the first explanation of nuclear fission in 1939 [1,2], a complete and unified understanding has not yet been achieved [3–5]. The LDM predicts only mass-symmetric fission of heavy nuclei, so the strongly mass-asymmetric fission of actinide nuclei requires inclusion of nuclear structure effects to explain its origin [6]. Initially, the observation of mass-asymmetric fission in the actinides was attributed to the influence of spherical proton and neutron shells in the nascent fragments [6,7]. However, a systematic experimental study performed in 2000 by Schmidt et al. that measured fragment charge distributions highlighted that *proton* shell effects appeared to be dominant in actinide fission [8]. A subsequent analysis performed by Bocksteigel et al., using the concept of independent fission channels, found the "standard I" and "standard II" modes to be centred at $Z = 52.5$ and 55 respectively [9]. Recent theoretical calculations have proposed that octupole deformations of fission fragments with Z = 52, 56 may be responsible for these two major mass-asymmetric fission modes of actinide nuclei [10].

Fission of nuclei lighter than the actinides had generally been believed to be predominantly mass-symmetric, in accordance with liquid drop model expectations. This picture changed following a challenging measurement of β-delayed fission, populating neutron-deficient ^{180}Hg at low-excitation energy E_x [11]. The mass yield was consistent with a single mass-asymmetric mode [11]. It was subsequently demonstrated through heavy-ion fusion reactions that the mass-asymmetric fission of ^{180}Hg persists to much higher excitation energy [12,13]. This opened up wide experimen-

* Corresponding author.
E-mail address: ben.swinton-bland@anu.edu.au (B.M.A. Swinton-Bland).
[1] Permanent address: Variable Energy Cyclotron Centre, 1/AF, Bidhan Nagar, Kolkata 700064, India.
[2] Present address: ACRF Image X Institute, University of Sydney, Central Clinical School, Sydney, Australia.

https://doi.org/10.1016/j.physletb.2022.137655

tal opportunities to investigate sub-lead fission using heavy-ion fusion [14–20]. Combined with theoretical predictions [21–25], a new perspective on nuclear fission is emerging.

Two key experimental and theoretical questions have arisen: how many fission modes are present in this mass region and what is the underlying physics responsible for these different modes? Modern experimental results from proton-bombardment reactions [26] and heavy-ion fusion reactions [15–17] have indicated the presence of at least one mass-symmetric and one mass-asymmetric fission mode in the sub-lead region. Recent investigations of the fission of neutron-deficient ^{178}Pt, however, disagree on the number of fission modes. Tsekhanovich et al. [15] proposed two distinct fission modes, one very low total kinetic energy (TKE) symmetric mode and one mass-asymmetric mode. Kozulin et al. [16] interpreted the fission of ^{178}Pt as a superposition of three asymmetric and one symmetric fission modes. Both investigations derive their interpretations from the analysis of discrete subsets (slices) of their measured data, either in fission fragment mass [16] or in the total kinetic energy spectrum [15], and integrate these results afterwards to form a whole picture of the reaction. This procedure creates a dependence of the final result on the subsets that are used, and due to low statistics in the measurements, has relied on systematics to constrain parameters [16].

To solve this disparity and determine independently the number and characteristics of the fission modes present in ^{178}Pt we have developed a new statistical fitting procedure that fits the full two-dimensional mass-kinetic energy distribution without external constraints or assumptions. This is combined with a new high-statistics, large-angular-coverage measurement of the fission of ^{178}Pt at an excitation energy (E_x = 37.7 MeV) lower than previously obtained.

2. Experiment

A beam of 146 MeV ^{34}S ions were delivered by the 14UD tandem accelerator at the Australian National University Heavy Ion Accelerator Facility. The beam impinged onto a $^{144}Sm_2O_3$ target, (96% isotopically enriched) with 86 µg cm^{-2} of Sm, sputtered onto a 36 µg cm^{-2} ^{nat}C backing which faced downstream to minimise energy loss of the fission fragments. Fission fragments were detected using the CUBE fission spectrometer, using three position sensitive multi-wire proportional counters (MWPCs), configured as shown in Ref. [27]. The kinematic coincidence method [28,29] was used to determine the mass ratio of the fission fragments, defined by $M_R = m_1/(m_1 + m_2)$ where $m_{1,2}$ represent the masses of the two fission fragments at scission. Energy-loss corrections were applied iteratively event-by-event. In total, 175 000 fission events were measured within an angular range $15° < \theta_{c.m.} < 165°$.

The measured mass-angle distribution (MAD) [29] is presented in Fig. 1, highlighting the large angular coverage of the CUBE fission spectrometer. There is no systematic change in mean fragment mass across the entire angular range, indicating no evidence for fast quasifission [29]. In the analysis, we first explore the information carried in the M_R distributions alone, before extending the analysis to the mass-TKE distribution. To avoid any biasing due to the detector angular acceptance, the fission fragment M_R distribution is obtained from the projection of the MAD from $90° \leq \theta_{c.m.} \leq 160°$ as shown by the black gate in Fig. 1. Thus, the M_R distribution is not mirrored about symmetry and therefore mass-asymmetric structure cannot be generated (or obscured) due to mis-calibration of the symmetry point. In addition, by using the directly measured mass-ratio instead of converting to atomic mass number, assumptions about pre-scission emission need not be made.

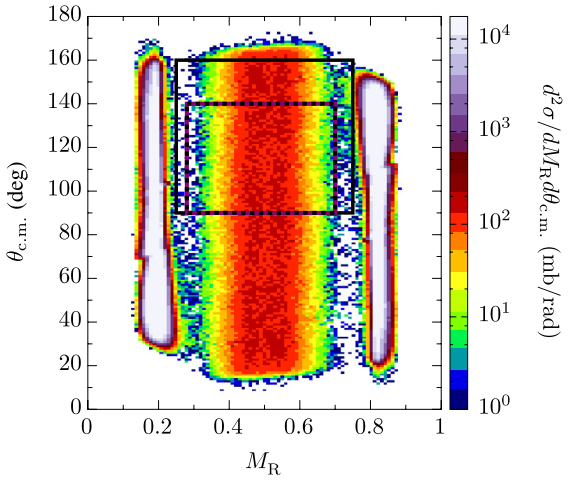

Fig. 1. The measured mass-angle distribution of the reaction ^{34}S + ^{144}Sm at centre-of-mass energy $E_{c.m.} = 117.6$ MeV. The intense regions around $M_R = 0.2$ and 0.8 are elastically scattered projectile and target nuclei, respectively. The fission events show no indication of a mass-angle correlation meaning there is no fast quasifission observed in this reaction. The black rectangular gate between $90° \leq \theta_{c.m.} \leq 160°$ is used for the projection of the fission fragment M_R distribution to avoid any angular biasing. The dashed purple-black rectangular gate is used for the two-dimensional fitting (see text).

3. Results

The extracted M_R distribution is presented in Fig. 2(a) (and repeated in Fig. 2(b)–Fig. 2(d)). It shows a strong two-peaked structure indicating that at least one mass-asymmetric fission mode must be present. To investigate whether there is only one or multiple asymmetric modes, the spectrum was fitted with multiple Gaussian functions. The asymmetric fission modes were defined as two identical Gaussians equidistant from the point of symmetry, whilst the symmetric fission mode (when included) was defined as a single Gaussian centred at the point of symmetry. As the mass distributions are not mirrored the symmetry point was included as a fitting parameter to account for small calibration offsets that may shift the mass distribution (typically less than 0.003 in M_R). For all fits, no parameters were fixed in the fitting routine, meaning no assumptions were made on the nature of the individual Gaussian components. The fit range was selected by investigating the M_R distribution in log-scale (Fig. 2(e)–(h)) to determine when the presence of projectile-like and target-like elastic contamination occurs, as shown by the filled points in Fig. 2(e)–Fig. 2(h). This allowed the widest fitting range to be determined, $0.28 \leq M_R \leq 0.70$.

Both the two- and three-Gaussian fits to the data, shown respectively in Fig. 2(a) and Fig. 2(b), fail to reproduce the structure observed in the measured distribution; confirmed by the large χ^2 per degree of freedom, χ^2_ν, values and clear structure in their residuals in Fig. 2(i) and Fig. 2(j), respectively. In contrast, the four-Gaussian fit does match the data well as seen in Fig. 2(c) and Fig. 2(g), with no obvious structure seen in the residuals (Fig. 2(k)) and a much-improved χ^2_ν value. The five-Gaussian fit is also a good representation of the data (Fig. 2(d), Fig. 2(h)), with residual structure (Fig. 2(l)) and χ^2_ν similar to the four-Gaussian fit. Higher order Gaussian fits were also performed in the analysis. Both six- and seven-Gaussian fits have higher χ^2_ν and result in one "mass-asymmetric" mode moving to symmetry, effectively producing a five-Gaussian fit. Therefore we conclude that there is no statistical justification for a higher number of Gaussian modes to fit the mass distribution of ^{178}Pt.

From the mass distribution alone we cannot distinguish between the viability of the four- and five-Gaussian fits, and therefore

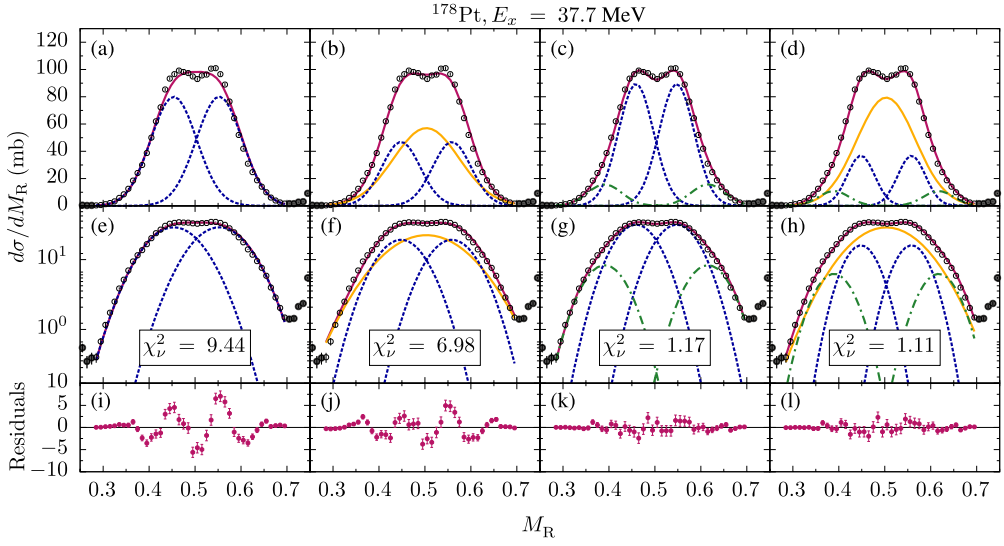

Fig. 2. Panels (a)–(d) show the measured fission fragment M_R distribution (hollow points) of ^{178}Pt at an excitation energy E_x = 37.7 MeV with two-, three-, four-, and five-Gaussian fits, respectively. The individual components of the total fit are also shown. Panels (e)–(h) show the measured M_R distribution and fits in log-scale. Regions which are contaminated by projectile-like and target-like elastics may be easily seen on this scale, and are shown by the filled points. The fitting region, as shown by the hollow points, is $0.28 \leq M_R \leq 0.70$. The χ^2 per degree of freedom χ^2_ν is presented for each fit. Panels (i)–(l) present the residuals from the respective fits. There is a clear and substantial improvement to the total fit with increasing number of Gaussians, with both four- and five-Gaussian fits being statistically similar.

cannot distinguish between two (four-Gaussian) or three (five-Gaussian) fission modes, but it is clear that a *minimum* of two asymmetric fission modes are required. Whilst statistically the four- and five-Gaussian fits are similar, the underlying physical interpretation is different. The four-Gaussian fit suggests the lack of a symmetric fission component, which would be surprising at this excitation energy.

To resolve the question of whether a mass-symmetric mode is present, and to discriminate between the four- and five-Gaussian representation, we investigate the total kinetic energy (TKE) of the fission fragments. Different fission modes can have different TKE if the fragment shapes at scission are different [4,33]. This additional information may allow clearer separation of the fission modes, and therefore clarify the most appropriate interpretation of the data. As the TKE is proportional to the square of the velocities of the two fission fragments, it is sensitive to any small differences in the measured timing signals between the two different detector pairs. For this reason, we only present TKE data from one detector pair, specifically the two large-area MWPCs spanning a centre-of-mass angle range $90° \leq \theta_{\text{c.m.}} \leq 140°$. This gate is shown on the MAD in Fig. 1 by the purple-dashed rectangle. This reduces the total counts used in the fitting procedure to 96 000.

The two-dimensional M_R-TKE plot is shown in Fig. 3(a) and shows the expected correlation of TKE with M_R. This correlation can be described by calculating the TKE through extension of the Viola systematics [30,31]:

$$\text{TKE}_{\text{Viola}} = \frac{0.755 Z_1 Z_2}{(A_1^{\frac{1}{3}} + A_2^{\frac{1}{3}})} + 7.3 \text{ MeV}. \quad (1)$$

The calculated $\text{TKE}_{\text{Viola}}$ for our measurement is shown by the black line in Fig. 3(a). To best extract information from both M_R and TKE, however, removal of this strong dependence on TKE with M_R is desirable. This can be achieved by determining the relative total kinetic energy (RTKE) [32]:

$$\text{RTKE} = \frac{\text{TKE}(M_R)}{\text{TKE}_{\text{Viola}}(M_R)}. \quad (2)$$

In determining $\text{TKE}_{\text{Viola}}(M_R)$, it is assumed that the fission fragments have the same N/Z ratio as that of the compound nucleus,

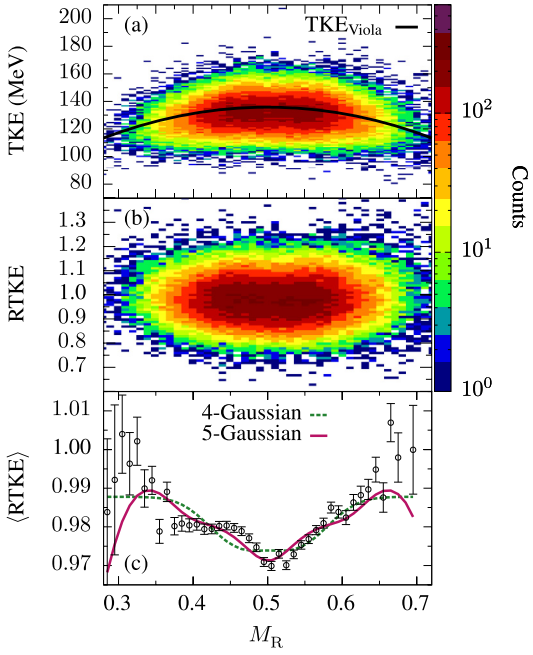

Fig. 3. Panel (a) shows the measured mass ratio (M_R) vs. total kinetic energy (TKE) of all fission fragments. The solid line shows the TKE from Viola Systematics [30,31]. Panel (b) shows the M_R vs the relative total kinetic energy (RTKE) [32] determined from the Viola Systematics. Panel (c) shows the average RTKE (⟨RTKE⟩) as a function of M_R. The noticeable dip at mass-symmetry in the ⟨RTKE⟩ indicates that a separate mass-symmetric fission mode is likely to be required in a two-dimensional fit. The dashed and solid lines correspond to the ⟨RTKE⟩ determined from the four- and five-Gaussian two-dimensional fits respectively (see text).

following the unchanged-charge-density (UCD) assumption [6]. The RTKE can be thought of as a proxy for the shape of the system at scission. The M_R-RTKE plot is shown in Fig. 3(b).

The linearisation of TKE by generating RTKE has two benefits. Firstly, the mean RTKE of *a given mode* is independent of M_R. Secondly, the width of the RTKE distribution can be taken as independent of M_R. This comes from the expectation [16] that the mass width for a given mode is proportional to TKE. Thus, each

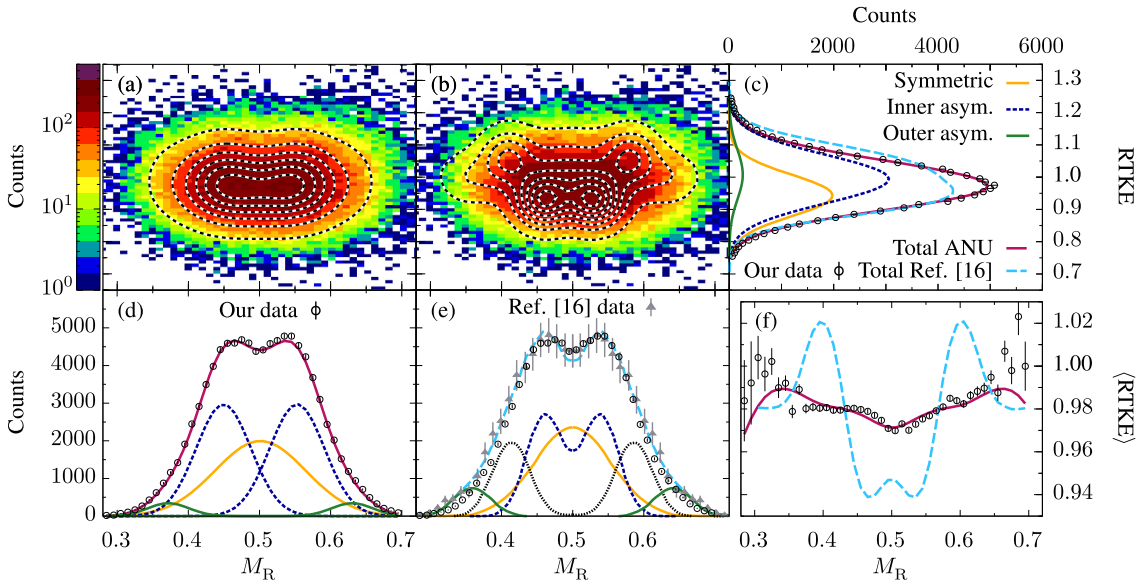

Fig. 4. Panel (a) presents M_R vs relative total kinetic energy (RTKE) (coloured histogram) with the two-dimensional five-Gaussian fit shown by the black and white contour lines. Panel (b) shows the same M_R vs RTKE histogram as panel (a), but with the combined one-dimensional interpretations (see text) of Ref. [16] represented by the black and white contours. Both sets of contour lines are set at the same levels across panels (a) and (b), which start at 20 and increment by 40 counts. The RTKE projection, with the total fit (maroon line) and individual components of the fit (multiple colours) is presented in panel (c), along with the reconstructed interpretation of Ref. [16] (light blue dashed-line). Panels (d) and (e) both present our M_R projection (hollow points) with our total fit and fit components shown in panel (d), and the scanned M_R distribution from Ref. [16] is shown in panel (e) by the grey triangles, with their determined fit and components. Panel (f) shows the measured average RTKE ($\langle$RTKE$\rangle$) as a function of M_R, along with both the five-Gaussian fit and the reconstructed interpretation of Ref. [16].

fission mode can be represented by a two-dimensional Gaussian in M_R vs. RTKE. Consequently, the *total* M_R-RTKE distribution can be described by a sum of two-dimensional Gaussian functions. This allows for simple two-dimensional fitting of the entire M_R-RTKE distribution, rather than applying either mass or TKE cuts and fitting slices of the distribution as previously used in fitting mass-TKE distributions of ^{178}Pt [15,16].

Both the four- and five-Gaussian two-dimensional fits were performed over the ranges $0.28 \leq M_R \leq 0.70$, as in the one-dimensional fitting range, and $0.75 \leq$ RTKE ≤ 1.25 to remove the influence of any low-intensity background events at extreme RTKE. The two-dimensional fitting procedure follows the same constraints as discussed for the one-dimensional M_R fitting. The five-Gaussian fit has $\chi^2_\nu = 1.10$, whilst the four-Gaussian fit has $\chi^2_\nu = 1.15$. In the two-dimensional distribution, it is difficult to compare visually the ability of these two fits to reproduce the data. This limitation can be overcome in this case by comparing the average RTKE, $\langle$RTKE$\rangle$, for each bin in M_R. This is presented in Fig. 3(c) and notably exhibits a sharp dip near mass-symmetry. The four-Gaussian two-dimensional fit (green-dashed line) does not reproduce this dip. In contrast the five-Gaussian fit (red line), which includes a mass-symmetric mode with a lower $\langle$RTKE$\rangle$, reproduces this feature. This is the clearest demonstration that the fission fragment distribution of ^{178}Pt is well described by the sum of three fission modes; one mass-symmetric, and two mass-asymmetric.

The total two-dimensional five-Gaussian fit to the M_R-RTKE distribution is presented in Fig. 4(a) as black and white contours overlaying the measured M_R-RTKE distribution. The projections and decompositions of the two-dimensional fit into both RTKE and M_R are shown in Fig. 4(c) and Fig. 4(d), respectively. Overall, the five-Gaussian two-dimensional fit is a good representation of the data, with strong agreement seen in both the M_R and RTKE distributions, and the contours in Fig. 4(a) matching well the shape of the measured two-dimensional distribution.

As was mentioned previously, there have been multiple studies of the fission of ^{178}Pt that have led to contrasting results. Both Tsekhanovich et al. [15] and Kozulin et al. [16] in the interpretations of their data applied gating of their measured two-dimensional mass-TKE distributions into either different TKE regions [15] or different mass regions [16]. Later investigations [14,16] failed to see any evidence of the claimed [15] low-energy component in the TKE distribution, which is also not seen in this work (see Fig. 4(c)).

The interpretation [16] of ^{178}Pt fission as having four fission modes differs from the results of the present analysis. To investigate this different conclusion, direct comparison between the current M_R distribution and that from Ref. [16] is made in Fig. 4(e). The latter data were scanned and converted from atomic mass to M_R and scaled to match the height of the peaks of our data. Overall, there is good agreement between the two data sets, especially near mass-symmetry, showing consistency between the two measurements. Minor differences, such as the wider distribution from Ref. [16], especially in the tails, may be due to the difference in excitation energy ($E_x = 37.7$ MeV for our measurement, $E_x = 42$ MeV in Ref. [16]) and/or the larger error bars resulting from the lower statistics obtained in Ref. [16] (estimated total of 1200 counts compared to 96 000 used in the two-dimensional fitting procedure in this work). The fit of Ref. [16] (scanned from Fig. 3 of Ref. [16] and shown by the blue-dashed line in Fig. 4) gives a reasonable description to the new high-statistics data also. The difference in interpretation must therefore lie in the TKE.

To allow full comparisons between the interpretation of the two-dimensional experimental results from this work and Ref. [16], the full M_R-RTKE distribution interpretation of the lowest energy measurement at $E_x = 42$ MeV [16] was reconstructed. The reconstruction used the tabulated Gaussian parameters for the four fission modes provided in Ref. [16] allowing generation of a mass-RTKE distribution for comparison with the present experimental results. Details on how this reconstruction was performed are given in the Supplementary Material.

The reconstructed one-dimensional RTKE distribution from the interpretation of Ref. [16] is presented in Fig. 4(c) by the blue-dashed line. The RTKE distributions show a notable difference, with our measured RTKE distribution (circles) being narrower and more peaked. This difference is likely due to the interpretation of Ref. [16] enforcing that their symmetric fission mode must have a

TKE equivalent to $\mathrm{TKE_{Viola}}$. This results in two narrow asymmetric fission modes at similar M_R but with very different RTKE, widening the distribution and reducing the sharpness of the peak, as discussed in more detail in the Supplementary Material. This suggests that whilst the TKE spectra for different mass ranges were well reproduced in Ref. [16], the total TKE distribution formed from these subsets possesses structure not observed in our high-statistics measurement.

This disagreement becomes much more apparent when looking at the two-dimensional M_R-RTKE distribution (Fig. 4(b)). The reconstructed four mode interpretation of Ref. [16] shares little resemblance with the current measurement, having substantially more structure. This is exemplified in the comparison of the ⟨RTKE⟩ of the four mode interpretation [16] (blue-dashed line) with our measured ⟨RTKE⟩ (hollow points) in Fig. 4(f), showing significant disagreement. The assumption of many fission modes with narrow mass and TKE distributions leads to much more structure in ⟨RTKE⟩ than is observed experimentally, and indicates that although fitting slices of one-dimensional projections can lead to good reconstruction of each slice, here it does not reproduce the actual structure observed in the full two-dimensional distribution. This highlights the importance of fitting directly the two-dimensional M_R-RTKE distribution to account for the experimentally observed structure.

The disagreement between the current measurement and the four mode interpretation of Ref. [16] raises an important question as to the validity of assuming that the symmetric fission mode will have a TKE equivalent to $\mathrm{TKE_{Viola}}$ as in Ref. [16]. If fission in this mass region largely results from shell effects that have different RTKE to the symmetric mode, it must be questioned whether $\mathrm{TKE_{Viola}}$ actually represents the liquid-drop model symmetric mode. If $\mathrm{TKE_{Viola}}$ represents the empirical average TKE, it should correspond to the average of all fission modes that are present.

Having determined that the fission of ^{178}Pt is most appropriately represented by three fission modes, we can investigate their M_R and RTKE centroids. For the three fission modes determined in this work, the M_R and RTKE centroids are tabulated in Table I in the Supplementary Material. The mass-symmetric fission mode has a lower RTKE (0.943 ± 0.003) than the two mass-asymmetric modes, which have comparable RTKE of 0.994 ± 0.002 for the inner mode and 1.008 ± 0.007 for the outer mode (uncertainties are purely statistical). These results suggest that the symmetric mode arises from a more elongated shape at scission than the two mass-asymmetric modes, discussed below.

To interpret the mass centroids in terms of shell structure, the M_R centroids of the two mass-asymmetric peaks can be converted to proton and neutron numbers following the UCD assumption [6], taking the N/Z ratio of the fission fragments to be the same as that of the ^{178}Pt compound nucleus. The determined proton numbers are 35.1 ± 0.1 and 42.9 ± 0.1 for the inner mode, and 29.0 ± 0.4 and 49.0 ± 0.4 for the outer mode and are presented in Fig. 5, whilst the neutron numbers are given in Table I in the Supplementary Material.

A recent measurement of fission of ^{178}Hg [18], formed in the ^{124}Xe + ^{54}Fe reaction, obtained the neutron-to-proton ratio (N/Z) of individual fission fragments. A consistent deviation from the UCD assumption was found for the light fragments. Given the proximity of ^{178}Pt and ^{178}Hg, and the similar excitation energies (37.7 and 34 MeV respectively), a similar deviation might be expected for ^{178}Pt. Ref. [18] noted that "the deviation … from UCD … does not affect significantly the transformation of the mass axis into the nuclear charge axis". To quantify this, we made use of the figures presented in Ref. [18], estimating a shift of ≤ 0.5 to the proton numbers of the fragments (lower for the light fragment, and higher for the heavy fragment). This small shift does not modify

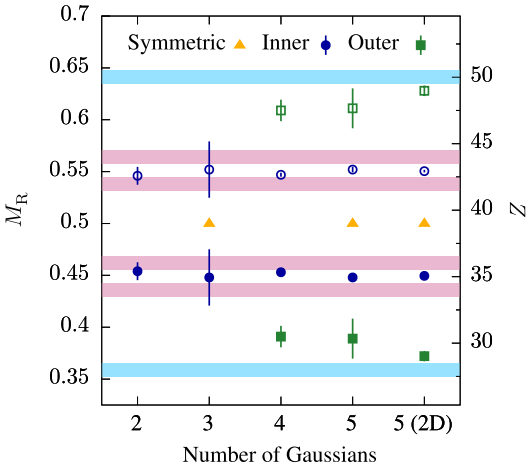

Fig. 5. Determined M_R centroids from two-, three-, four-, and five-Gaussian one-dimensional fits for the light (filled points) and heavy (hollow points) fission fragments. The M_R centroids determined from the five-Gaussian two-dimensional fit are also presented. Corresponding proton numbers Z, for each centroid are also shown on the right, determined using the UCD assumption (see text). Expected quadrupole deformed shell gaps at $Z = 34, 36$ for the light fragments (solid points) and $Z = 42, 44$ for the heavy fragments (hollow points) are shown by the pink bands. Spherical proton shell gaps at $Z = 28, 50$ are highlighted by the pale blue bands.

our final conclusions, so to avoid introducing additional uncertainties, we have continued to use the UCD assumption. This issue is discussed in more detail in the Supplementary Material.

Focussing initially on the inner mass-asymmetric mode, the proton and neutron numbers are similar to those previously found experimentally [14,19] for ^{178}Pt. In addition, they are similar to those predicted by microscopic calculations from the work of Scamps and Simenel [21]. Scamps and Simenel attribute mass-asymmetric fission to the influence of an octupole deformed shell gap at $N = 56$, as well as noting the possible influence of proton and neutron shell gaps arising from large quadrupole shell gaps at $Z = 34, 44$ and $N = 44, 46$ that would be present in an elongated fragment [21]. These calculations have shown strong agreement with systematic measurements in the sub-lead region [14], as well as the current results. However, they predict only one mass-asymmetric fission mode for ^{178}Pt and do not account for the observed outer mass-asymmetric mode. It is worth noting that the calculations from Ref. [21] have the ability to predict two mass-asymmetric modes of fission, as found for ^{190,192,194}Hg.

The outer mass-asymmetric fission mode is situated close to both the $Z = 28$ and $Z = 50$ spherical closed shells. However, experimentally the RTKE of this mode is similar to that of the inner mass-asymmetric mode, which is attributed to deformed shell gaps. This would suggest that if the closed shells do in fact play a role in this outer asymmetric mode, *both* cannot contribute to this mode, otherwise the RTKE would be expected to be far larger due to the combination of two compact fission fragments (as seen in the fission of fermium isotopes [34]). If only one of the spherical shells were influencing this mode, the complementary fragment would be required to have a very large elongation.

It is important to note the stability of the inner-asymmetric mode centroid as the number of Gaussians used to fit the distribution is increased. The deduced M_R centroids from each fit are presented in Fig. 5. It is clear that the inner asymmetric mode remains consistent across the different fits. The inner mode centroid is also in good agreement with lower-statistics measurements in this mass region [14,16,19,20]. This indicates that the presence and location of this mode can be well determined in lower-statistics measurements as long as the excitation energy is sufficiently low to allow structure to be seen in the mass distribu-

tion [12,13,16,18,26]. However, to unambiguously show the presence of a second, weaker mass-asymmetric mode, at larger mass-asymmetry, it is clear that high-statistics measurements, such as the one presented in this Letter, are necessary.

4. Conclusions

In this Letter, we have presented a high-statistics, wide-angular coverage measurement of the fission of ^{178}Pt at an excitation energy ($E_x = 37.7$ MeV) 4 MeV lower than previous measurements [15,16]. We have combined high statistics data with a new rigorous statistical analysis procedure. This shows, without assumption or fixing of any fitting parameters, that the fission distribution of ^{178}Pt can be represented by three distinct fission modes, one mass-symmetric and two mass-asymmetric. Comparison with previous approaches shows the necessity of two-dimensional fitting of mass and kinetic energy (either total or relative) to properly interpret the measured distributions. The mass-symmetric fission mode is determined to have a substantially lower RTKE than the two mass-asymmetric fission modes, which have comparable RTKE. The inner mass-asymmetric fission mode is consistent with theoretical calculations [21] and previous experimental investigations [14,16,18,19], and is attributed to an elongated shape at scission. The outer mass-asymmetric fission mode has similar RTKE as the inner mode despite the Z values being close to spherical closed shells at $Z = 28$ and $Z = 50$. If one of these shells were responsible for this outer mode, the complementary fragment would be expected to very deformed. To quantify this statement, however, theoretical calculations that connect deformation and TKE quantitatively are required. Future high-statistics systematic studies, combined with a rigorous statistical analysis, as performed here, are required to determine definitively which shell effects are responsible for the observed mass-asymmetric fission modes in sub-lead nuclei. Theoretical investigations in the sub-lead region must be able to predict the presence of two mass-asymmetric fission modes and their respective TKEs.

Declaration of competing interest

The authors declare that they have no known competing financial interests or personal relationships that could have appeared to influence the work reported in this paper.

Data availability

Data will be made available on request.

Acknowledgements

The authors acknowledge support from the Australian Research Council through Discovery Grants No. DP170102318, No. DP190101442, DP190100256, and No. DP200100601. Support for the ANU Heavy Ion Accelerator Facility operations from the Australian National Collaborative Research Infrastructure (NCRIS) HIA project is acknowledged. Work at Lawrence Livermore National Laboratory (LLNL) was performed under the auspices of the U.S. Department of Energy by LLNL under Contract No. DE-AC52-07NA27344. B. M. A. S-B, J. B, and L. T. B. acknowledge the support of the Australian Government Research Training Program.

Appendix A. Supplementary material

Supplementary material related to this article can be found online at https://doi.org/10.1016/j.physletb.2022.137655.

References

[1] N. Bohr, J.A. Wheeler, The mechanism of nuclear fission, Phys. Rev. 56 (1939) 426–450, https://doi.org/10.1103/PhysRev.56.426.
[2] L. Meitner, O.R. Frisch, Disintegration of uranium by neutrons: a new type of nuclear reaction, Nature 143 (3615) (1939) 239–240, https://doi.org/10.1038/143239a0.
[3] K.-H. Schmidt, B. Jurado, Review on the progress in nuclear fission—experimental methods and theoretical descriptions, Rep. Prog. Phys. 81 (10) (2018) 106301, https://doi.org/10.1088/1361-6633/aacfa7.
[4] A.N. Andreyev, K. Nishio, K.-H. Schmidt, Nuclear fission: a review of experimental advances and phenomenology, Rep. Prog. Phys. 81 (1) (2017) 016301, https://doi.org/10.1088/1361-6633/aa82eb.
[5] M. Bender, R. Bernard, G. Bertsch, S. Chiba, J. Dobaczewski, N. Dubray, S.A. Giuliani, K. Hagino, D. Lacroix, Z. Li, et al., Future of nuclear fission theory, J. Phys. G, Nucl. Part. Phys. 47 (11) (2020) 113002, https://doi.org/10.1088/1361-6471/abab4f.
[6] R. Vandenbosch, J.R. Huizenga, Nuclear Fission, Academic Press, New York, 1973.
[7] L. Meitner, Fission and nuclear shell model, Nature 165 (4197) (1950) 561, https://doi.org/10.1038/165561a0.
[8] K.-H. Schmidt, S. Steinhäuser, C. Böckstiegel, A. Grewe, A. Heinz, A.R. Junghans, J. Benlliure, H.-G. Clerc, M. De Jong, J. Müller, M. Pfützner, B. Voss, Relativistic radioactive beams: a new access to nuclear-fission studies, Nucl. Phys. A 665 (3–4) (2000) 221–267, https://doi.org/10.1016/S0375-9474(99)00384-X.
[9] C. Böckstiegel, S. Steinhäuser, K.-H. Schmidt, H.-G. Clerc, A. Grewe, A. Heinz, M. de Jong, A.R. Junghans, J. Müller, B. Voss, Nuclear-fission studies with relativistic secondary beams: analysis of fission channels, Nucl. Phys. A 802 (1–4) (2008) 12–25, https://doi.org/10.1016/j.nuclphysa.2008.01.012.
[10] G. Scamps, C. Simenel, Impact of pear-shaped fission fragments on mass-asymmetric fission in actinides, Nature 564 (7736) (2018) 382–385, https://doi.org/10.1038/s41586-018-0780-0.
[11] A.N. Andreyev, J. Elseviers, M. Huyse, P. Van Duppen, S. Antalic, A. Barzakh, N. Bree, T.E. Cocolios, V.F. Comas, J. Diriken, D. Fedorov, V. Fedosseev, S. Franchoo, J.A. Heredia, O. Ivanov, U. Köster, B.A. Marsh, K. Nishio, R.D. Page, N. Patronis, M. Seliverstov, I. Tsekhanovich, P. Van den Bergh, J. Van De Walle, M. Venhart, S. Vermote, M. Veselsky, C. Wagemans, T. Ichikawa, A. Iwamoto, P. Möller, A.J. Sierk, New type of asymmetric fission in proton-rich nuclei, Phys. Rev. Lett. 105 (2010) 252502, https://doi.org/10.1103/PhysRevLett.105.252502.
[12] E. Prasad, D.J. Hinde, K. Ramachandran, E. Williams, M. Dasgupta, I.P. Carter, K.J. Cook, D.Y. Jeung, D.H. Luong, S. McNeil, et al., Observation of mass-asymmetric fission of mercury nuclei in heavy ion fusion, Phys. Rev. C 91 (6) (2015) 064605, https://doi.org/10.1103/PhysRevC.91.064605.
[13] K. Nishio, A.N. Andreyev, R. Chapman, X. Derkx, C.E. Düllmann, L. Ghys, F.P. Heßberger, K. Hirose, H. Ikezoe, J. Khuyagbaatar, et al., Excitation energy dependence of fragment-mass distributions from fission of ^{180,190}Hg formed in fusion reactions of ^{36}Ar $+^{144,154}$ Sm, Phys. Lett. B 748 (2015) 89–94, https://doi.org/10.1016/j.physletb.2015.06.068.
[14] E. Prasad, D.J. Hinde, M. Dasgupta, D.Y. Jeung, A.C. Berriman, B.M.A. Swinton-Bland, C. Simenel, E.C. Simpson, R. Bernard, E. Williams, et al., Systematics of the mass-asymmetric fission of excited nuclei from ^{176}Os to ^{206}Pb, Phys. Lett. B 811 (2020) 135941, https://doi.org/10.1016/j.physletb.2020.135941.
[15] I. Tsekhanovich, A.N. Andreyev, K. Nishio, D. Denis-Petit, K. Hirose, H. Makii, Z. Matheson, K. Morimoto, K. Morita, W. Nazarewicz, R. Orlandi, J. Sadhukan, T. Tanaka, M. Vermeulen, M. Warda, Observation of the competing fission modes in ^{178}Pt, Phys. Lett. B 790 (2019) 583–588, https://doi.org/10.1016/j.physletb.2019.02.006.
[16] E.M. Kozulin, G.N. Knyazheva, I.M. Itkis, M.G. Itkis, Y.S. Mukhamejanov, A.A. Bogachev, K.V. Novikov, V.V. Kirakosyan, D. Kumar, T. Banerjee, M. Cheralu, M. Maiti, R. Prajapat, R. Kumar, G. Sarkar, W.H. Trzaska, A.N. Andreyev, I.M. Harca, A. Mitu, E. Vardaci, Fission of ^{180,182,183}Hg* and ^{178}Pt* nuclei at intermediate excitation energies, Phys. Rev. C 105 (2022) 014607, https://doi.org/10.1103/PhysRevC.105.014607.
[17] A. Bogachev, E. Kozulin, G. Knyazheva, I. Itkis, M. Itkis, K. Novikov, D. Kumar, T. Banerjee, I. Diatlov, M. Cheralu, et al., Asymmetric and symmetric fission of excited nuclei of ^{180,190}Hg and ^{184,192,202}Pb formed in the reactions with ^{36}Ar and ^{40,48}Ca ions, Phys. Rev. C 104 (2) (2021) 024623, https://doi.org/10.1103/PhysRevC.104.024623.
[18] C. Schmitt, A. Lemasson, K.-H. Schmidt, A. Jhingan, S. Biswas, Y. Kim, D. Ramos, A. Andreyev, D. Curien, M. Ciemala, et al., Experimental evidence for common driving effects in low-energy fission from sublead to actinides, Phys. Rev. Lett. 126 (13) (2021) 132502, https://doi.org/10.1103/PhysRevLett.126.132502.
[19] K. Mahata, C. Schmitt, S. Gupta, A. Shrivastava, G. Scamps, K.-H. Schmidt, Evidence for the general dominance of proton shells in low-energy fission, Phys. Lett. B 825 (2022) 136859, https://doi.org/10.1016/j.physletb.2021.136859.
[20] T. Nag, R. Tripathi, S. Patra, A. Mhatre, S. Santra, P. Rout, A. Kundu, D. Chattopadhyay, A. Pal, P. Pujari, Fission fragment mass distribution in the ^{32}S $+^{144}$ Sm reaction, Phys. Rev. C 103 (3) (2021) 034612, https://doi.org/10.1103/PhysRevC.103.034612.

[21] G. Scamps, C. Simenel, Effect of shell structure on the fission of sub-lead nuclei, Phys. Rev. C 100 (2019) 041602(R), https://doi.org/10.1103/PhysRevC.100.041602.

[22] P. Möller, J. Randrup, A.J. Sierk, Calculated fission yields of neutron-deficient mercury isotopes, Phys. Rev. C 85 (2) (2012) 024306, https://doi.org/10.1103/PhysRevC.85.024306.

[23] J.D. McDonnell, W. Nazarewicz, J.A. Sheikh, A. Staszczak, M. Warda, Excitation-energy dependence of fission in the mercury region, Phys. Rev. C 90 (2014) 021302(R), https://doi.org/10.1103/PhysRevC.90.021302.

[24] A.V. Andreev, G.G. Adamian, N.V. Antonenko, Asymmetry of fission fragment mass distribution for Po and Ir isotopes, Phys. Rev. C 93 (2016) 034620, https://doi.org/10.1103/PhysRevC.93.034620.

[25] H. Paşca, A.V. Andreev, G.G. Adamian, N.V. Antonenko, Examination of coexistence of symmetric mass and asymmetric charge distributions of fission fragments, Phys. Rev. C 101 (2020) 064604, https://doi.org/10.1103/PhysRevC.101.064604.

[26] B.M.A. Swinton-Bland, M.A. Stoyer, A.C. Berriman, D.J. Hinde, C. Simenel, J. Buete, T. Tanaka, K. Banerjee, L.T. Bezzina, I.P. Carter, K.J. Cook, M. Dasgupta, D.Y. Jeung, C. Sengupta, E.C. Simpson, K. Vo-Phuoc, Mass-asymmetric fission of ^{205,207,209}Bi at energies close to the fission barrier using proton bombardment of ^{204,206,208}Pb, Phys. Rev. C 102 (2020) 054611, https://doi.org/10.1103/PhysRevC.102.054611.

[27] T. Banerjee, D.J. Hinde, D.Y. Jeung, K. Banerjee, M. Dasgupta, A.C. Berriman, L.T. Bezzina, H.M. Albers, C.E. Düllmann, J. Khuyagbaatar, B. Kindler, B. Lommel, E.C. Simpson, C. Sengupta, B.M.A. Swinton-Bland, T. Tanaka, A. Yakushev, K. Eberhardt, C. Mokry, J. Runke, P. Thörle-Pospiech, N. Trautmann, Systematic evidence for quasifission in ^{9}Be−, ^{12}C−, and ^{16}O-induced reactions forming ^{258,260}No, Phys. Rev. C 102 (2020) 024603, https://doi.org/10.1103/PhysRevC.102.024603.

[28] D.J. Hinde, M. Dasgupta, J.R. Leigh, J.C. Mein, C.R. Morton, J.O. Newton, H. Timmers, Conclusive evidence for the influence of nuclear orientation on quasifission, Phys. Rev. C 53 (1996) 1290–1300, https://doi.org/10.1103/PhysRevC.53.1290.

[29] R. du Rietz, E. Williams, D.J. Hinde, M. Dasgupta, M. Evers, C.J. Lin, D.H. Luong, C. Simenel, A. Wakhle, Mapping quasifission characteristics and timescales in heavy element formation reactions, Phys. Rev. C 88 (2013) 054618, https://doi.org/10.1103/PhysRevC.88.054618.

[30] V.E. Viola, K. Kwiatkowski, M. Walker, Systematics of fission fragment total kinetic energy release, Phys. Rev. C 31 (1985) 1550–1552, https://doi.org/10.1103/PhysRevC.31.1550.

[31] J. Tōke, R. Bock, G.X. Dai, A. Gobbi, S. Gralla, K.D. Hildenbrand, J. Kuzminski, W.F.J. Müller, A. Olmi, H. Stelzer, B.B. Back, S. Bjørnholm, Quasi-fission—the mass-drift mode in heavy-ion reactions, Nucl. Phys. A 440 (2) (1985) 327–365, https://doi.org/10.1016/0375-9474(85)90344-6.

[32] D.J. Hinde, D. Hilscher, H. Rossner, B. Gebauer, M. Lehmann, M. Wilpert, Neutron emission as a probe of fusion-fission and quasifission dynamics, Phys. Rev. C 45 (3) (1992) 1229, https://doi.org/10.1103/PhysRevC.45.1229.

[33] T. Ichikawa, A. Iwamoto, P. Möller, A.J. Sierk, Contrasting fission potential-energy structure of actinides and mercury isotopes, Phys. Rev. C 86 (2) (2012) 024610, https://doi.org/10.1103/PhysRevC.86.024610.

[34] E. Hulet, J. Wild, R. Dougan, R. Lougheed, J. Landrum, A. Dougan, M. Schadel, R. Hahn, P. Baisden, C. Henderson, et al., Bimodal symmetric fission observed in the heaviest elements, Phys. Rev. Lett. 56 (4) (1986) 313, https://doi.org/10.1103/PhysRevLett.56.313.